Polymer 50 (2009) 5134–5141

Contents lists available at ScienceDirect

Polymer

journal homepage: www.elsevier.com/locate/polymer

Morphology of polypropylene/poly(ethylene-*co*-propylene) in-reactor alloys prepared by multi-stage sequential polymerization and two-stage polymerization

Ying Li [a], Jun-Ting Xu [a,b,*], Qi Dong [a], Zhi-Sheng Fu [a], Zhi-Qiang Fan [a,b]

[a] MOE Key Laboratory of Macromolecular Synthesis and Functionalization, Department of Polymer Science & Engineering, Zhejiang University, 38 Zheda Road, Hangzhou, Zhejiang 310027, China
[b] State Key Laboratory of Chemical Engineering, Department of Chemical and Biological Engineering, Zhejiang University, Hangzhou 310027, China

ARTICLE INFO

Article history:
Received 27 May 2009
Received in revised form
31 August 2009
Accepted 3 September 2009
Available online 11 September 2009

Keywords:
Crystallization
Phase separation
Polypropylene

ABSTRACT

The morphology of two polypropylene/poly(ethylene-*co*-propylene) (PP/EPR) in-reactor alloys prepared by multi-stage sequential polymerization (MSSP) and two-stage polymerization (TSP) processes, respectively, was investigated. It is observed that the alloy prepared by MSSP (sample 1) exhibits lower phase separation temperature than the alloy prepared by TSP (sample 2), probably due to the higher content of PP segments in the blocky copolymer fractions of sample 1. Two thermal treatments were applied to the samples: (1) The samples were directly quenched from 230 °C to 132 °C for isothermal crystallization; (2) The samples were firstly held at 160 °C for 60 min for phase separation and then cooled to 132 °C for crystallization. It is found that both microstructure and thermal treatment affect the morphology of the alloys, and the differences in morphology are interpreted in terms of phase diagram. For sample 1 and for the samples subjected to phase separation prior to crystallization, the EPR-rich phase contains more PP and thus is more viscous, which leads to more inclusion of the EPR-rich phase into the spherulites. A coarse spherulitic structure is formed due to crystallization of PP in the included EPR-rich phase. More included EPR-rich phase and its stronger crystallizability can further lead to the narrower boundaries and formation of connections between the adjacent spherulites.

1. Introduction

As is well-known, in-reactor blending, which involves homopolymerization of propylene followed by copolymerization of ethylene and propylene, can significantly improve the poor low temperature impact properties of polypropylene (PP) [1–3]. The so-called polypropylene/poly(ethylene-*co*-propylene) (PP/EPR) in-reactor alloy is now mainly produced by a two-stage polymerization (TSP) process. In the first stage, propylene homopolymerization is performed in the presence of a spherical $TiCl_4/MgCl_2$-based catalyst and porous PP particles were produced. In the second stage, ethylene–propylene copolymerization occurs and a rubbery EPR phase was prepared and incorporated into the pre-formed PP matrix [4–7]. It has been demonstrated that the PP/EPR alloy possesses excellent impact strength, in comparison to mechanical blends of PP/EPR, benefited from its unique morphology [8–16] and special components such as ethylene–propylene blocky copolymer [17–19]. Recently a new process for producing PP in-reactor alloy based on multi-zone circulating reactor (MZCR) was reported [20–23]. In this process, the polymer granules are rapidly circulated between a reaction zone containing pure propylene and a reaction zone where a mixture of ethylene and propylene is fed. This means that the retention time of the polymer granules in each homopolymerization and copolymerization stage is very short, while the whole polymerization time is still long enough to reach a high polymer yield. The switch frequency between homopolymerization and copolymerization stages can be regulated by changing the retention time in these two reaction zones. We simulated such a polymerization process and prepared two PP/EPR alloys by multi-stage sequential gas-phase homopolymerization of propylene and gas-phase ethylene–propylene copolymerization in a circular mode [24]. The switch times between homopolymerization and copolymerization stages is 8 and 1 for sample 1 and sample 2, respectively, and the total time for homopolymerization and copolymerization maintains the same for both samples. It should be noticed that sample 2 could be well representative of in-reactor alloy produced by conventional two-step process (TSP). We found that, when the switch frequency between homopolymerization and copolymerization increased, the dimension of EPR phase decreased and the size distribution of the dispersed EPR phase became more uniform, but

* Corresponding author at: MOE Key Laboratory of Macromolecular Synthesis and Functionalization, Department of Polymer Science & Engineering, Zhejiang University, 38 Zheda Road, Hangzhou, Zhejiang 310027, China. Tel./fax: +86 571 87952400.
E-mail address: xujt@zju.edu.cn (J.-T. Xu).

0032-3861/$ – see front matter © 2009 Elsevier Ltd. All rights reserved.
doi:10.1016/j.polymer.2009.09.008

the total EPR content in the in-reactor alloys was hardly influenced [24]. The PP/EPR in-reactor alloy prepared by MSSP exhibits better mechanical properties in both impact strength and flexural modulus tests than PP/EPR alloy produced by conventional two-stage polymerization process. So far most reports focused on the relationship between structure and properties of PP/EPR alloys prepared by two-stage polymerization [25–28], but very few on PP/EPR alloys prepared by MSSP or MCZR.

On the other hand, the PP/EPR alloy is a mixture, which contains crystalline PP homopolymer, amorphous EPR, blocky and/or segmented ethylene–propylene copolymers [29–31]. For a blend containing both crystalline and amorphous components, the ultimate morphology and mechanical properties strongly depend on thermal treatment due to the interplay of phase separation and crystallization. It has been demonstrated that crystallization kinetic and morphology of crystalline/amorphous polymer blends are affected by the rates of crystallization and phase separation, size of the phase-separated domains, crystallization temperature, temperature and time for phase separation and other factors [32–47].

In the present work, we compared the morphologies of two PP/EPR alloys prepared by TSP and MSSP, respectively, under different thermal treatments, and the differences were interpreted in terms of structure and phase diagram. The aim of this preliminary study work is to reveal how the morphology of PP/EPR in-situ alloys can be controlled by regulation of polymerization process (or microstructure of the alloys) and interplay of phase separation and crystallization.

2. Experimental

2.1. Preparation of PP/EPR in-reactor alloys

Details for preparation of PP/EPR in-reactor alloys were described in reference [24]. A multi-stage sequential polymerization process was conducted using a high yield spherical Ziegler-Natta catalyst, $TiCl_4/MgCl_2 \cdot ID$ (where ID is an internal donor), kindly donated by BRICI, SINOPEC (Beijing, China). In the first stage, propylene homopolymerization was carried out for 60 min after the prepolymerization conducted in a well-stirred glass reactor. Next is a circular reaction mode including ethylene–propylene copolymerization, in which an ethylene–propylene mixture of a constant composition (propylene/ethylene = 1.5) was continuously supplied to the autoclave under constant pressure (0.4 MPa), and propylene homopolymerization under constant pressure (0.6 MPa). That is to say, after ethylene–propylene copolymerization for a designed time, the polymerization was switched to propylene homopolymerization and subsequently ethylene–propylene copolymerization at the same conditions as above. The circular reaction mode was carried out for 80 min at 60 °C. In the circular reaction, sample 2 was prepared by ethylene–propylene copolymerization for 20 min and then propylene homopolymerization for 60 min, namely, the switch times of sample 2 was 1. Analogically, sample 1 was synthesized by ethylene–propylene copolymerization for 2.5 min and then propylene homopolymerization for 7.5 min in a circle and its switch times was 8. It is noteworthy that compared to sample 1 prepared by MSSP process, sample 2 is actually prepared by the conventional TSP process. The polymerization parameters and mechanical properties of both samples are given in Table 1.

2.2. Thermal fractionation

About 5 mg of each sample was sealed in an aluminum pan and subjected to stepwise isothermal crystallization according to the following procedure: The samples were first heated to 200 °C under nitrogen atmosphere and held for 100 min to erase the thermal history. Then the samples were cooled down to the first isothermal crystallization temperature ($T_{c1} = 130$ °C) and held at this temperature for 12 h, and then successively cooled down to a series of isothermal crystallization temperatures (T_c) set at 125, 120, 115, 110, 105, 100, 95, 90, 85, 80, 75, 70, 65, and 60 °C, respectively, and held at each temperature for 12 h. This temperature difference (5 °C) is defined as the "fractionation window". The melting endotherms of the samples after step crystallization were recorded on a Perkin-Elmer Pyris-1 calorimeter at a heating rate of 10 °C/min from 30 to 200 °C. In the other procedure, a "fractionation window" of 10 °C and holding time of 24 h at each T_c were employed as well.

2.3. Optical microscopy

Polarized optical microscopy (POM) observations were carried out on an Olympus BX-51 polarized optical microscope (Tokyo, Japan) equipped with a hot-stage and a digital camera. A small piece of sample placed between two cover glasses was first melted at 230 °C for 10 min on the hot-stage and the thermal history of the sample was erased, and then morphology during isothermal crystallization was observed. Two different thermal treatments were applied to the samples prior to isothermal crystallization. In the first thermal treatment, the samples were cooled directly from 230 °C to 132 °C at a rate of 30 °C/min to complete isothermal crystallization. In the second thermal treatment, the samples were firstly quenched from 230 °C to 160 °C and held for 60 min to facilitate phase separation, and then cooled to 132 °C at a rate of 30 °C/min for isothermal crystallization. The samples in POM experiments were also used for phase contrast optical microscopy (PCOM) observations, which were carried out on phase contrast microscope (XSZ-HX, Chongqing, China) equipped with a JVC color video camera (TK-C921EC).

2.4. Scanning electron microscopy (SEM)

The morphology of spherulites was investigated using a scanning electron microscope (FEI-SIRION). The SEM samples were prepared as follows: films of sample 1 and sample 2 were placed between two cover glasses on the hot-stage of the above-mentioned Olympus BX-51 optical microscope (Tokyo, Japan), and first melted at 230 °C for 10 min to erase the thermal history of samples. Then two different thermal treatments as described in Section 2.3 were applied to the films before isothermal crystallization at 132 °C. The film was then etched by xylene for 24 h at room temperature to remove non-crystalline ethylene–propylene random copolymer and then coated with gold before observation.

Table 1
Polymerization conditions and mechanical properties of two PP/EPR in-reactor alloys.

Sample	Retention time in each polymerization cycle (min)		Switch number (times)	Impact strength (KJ/m^2)	Flexural modulus (MPa)
	Propylene homopolymerization	Ethylene–propylene copolymerization			
Sample 1	2.5	7.5	8	13.6	915.7
Sample 2	20	60	1	3.9	770.7

2.5. Small-angle light scattering (SALS)

The small-angle light scattering (SALS) apparatus was described in reference [48]. A He–Ne laser generator was used as the incident beam with the wavelength of 632.8 nm. The temperature accuracy of the hot-stage controlled by an intelligent controller (AI-708, Yuguang, China) was about ±0.1 °C. The scattering pattern was detected by a CCD digital camera (MTV-12V1C, Mintron, Taiwan) and the data were imported into the computer memory in real time through a video capturing board (VIDEO VESA CG-400, Daheng, China). Online circular averaging of each scattering pattern was performed to obtain the SALS intensity. The film samples were firstly heated to 230 °C and hold for 5 min, then cooled to 140 °C at a rate of 0.5 °C/min. The SALS intensities were measured upon cooling.

3. Results

3.1. Thermal fractionation and phase separation temperature

The DSC melting curves of sample 1 and sample 2 after stepwise crystallization fractionation with a fractionation window of 5 °C are shown in Fig. 1. However, the DSC peaks at low temperature range are very weak under such a thermal fractionation condition. In order to reveal the DSC peaks at low temperature range clearly, stepwise crystallization fractionation was also conducted at a fractionation window of 10 °C, and the corresponding DSC melting curves in low temperature range are inserted in Fig. 1. There are two major peaks at high temperature range together with many weak peaks at low temperature range for both samples. Comparing the relative intensities of the DSC melting peaks, one can see that relative intensity of the melting peaks at 140 °C is stronger in sample 1 than that in sample 2. This peak is attributed to the melting of blocky ethylene–propylene copolymers. The crystalline PP segments in the blocky copolymer fractions are chemically linked with other segments (such as ethylene–propylene random copolymer segments), leading to the lower melting temperature of PP segments [17,49]. However, our previous temperature rising elution fractionation result showed that these two samples had similar weight percentages of EPR content (eluted at room temperature) and blocky copolymer (eluted between 30 and 100 °C) [24]. As a result, the different thermal fractionation curves of sample 1 and sample 2 are probably due to the different compositions of the blocky fractions. The higher intensity of the shoulder peak at 140 °C indicates that the blocky fractions of the PP/EPR in-reactor alloy sample 1 prepared by MSSP contain more PP segments than the blocky fractions in sample 2 prepared by TSP. To exclude possible influences of the phase dispersion states, we dissolved these two samples in xylene and found that the recovered samples still exhibited different thermal behaviors. This means that the smaller size of EPR phase in sample 1 than in sample 2 [24] is not the main reason for their different thermal behaviors. There must be some differences in chain structure between the two samples.

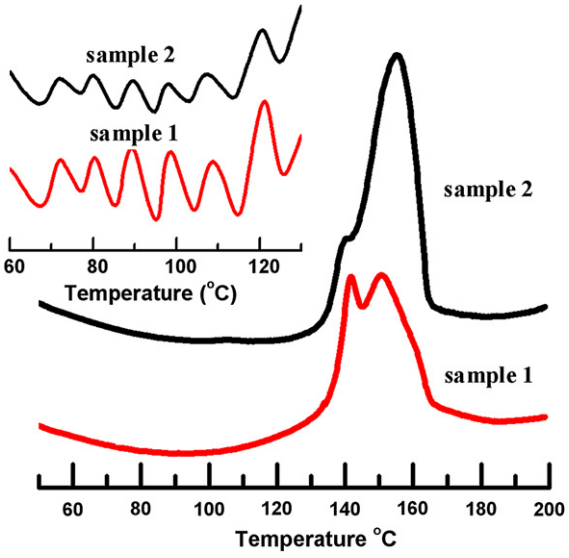

Fig. 1. DSC melting curves of sample 1 and sample 2 after stepwise crystallization fractionation with a fractionation window of 5 °C. Inset is the DSC melting curves in low temperature region after stepwise crystallization fractionation with a fractionation window of 10 °C.

The difference in structure between sample 1 and sample 2 will inevitably lead to their different phase behaviors. Fig. 2 shows the variations of SALS intensity with temperature for sample 1 and sample 2. Since PP and EPR have similar refractive indices, it is difficult to get good result from the SALS experiments. This lead to the noisy data in Fig. 2, but we still can see a transition occurs upon cooling. At high temperature the alloys are homogeneous and the SALS intensity nearly keeps constant. As phase separation takes place, the SALS intensity increases gradually with decrease in temperature. The phase separation temperatures are 182 °C and 205 °C for sample 1 and sample 2, respectively. The blocky copolymer of polypropylene-*b*-poly(ethylene-*co*-propylene) can act as compatilizer of PP and EPR. In sample 1 the blocky fractions have better compatibility with PP due to higher content of PP segments, leading to its lower phase separation temperature. It should be noted that there are still controversies about the phase diagram of PP/EPR binary blends. A lower critical solution temperature (LCST) type phase diagram was observed by some authors [37,50], but others believed the phase diagram of PP/EPR binary blends is upper critical solution temperature (UCST) type [34,51]. Also Seki et al. reported that PP and EPR were miscible in the melt [52]. Our result indicates that the phase diagram of PP/EPR in-reactor alloys is UCST type in the presence of propylene/ethylene-*co*-propylene blocky copolymers.

3.2. Optical microscopy

In order to investigate the effect of the interplay of phase separation and crystallization on morphology of PP/EPR in-reactor

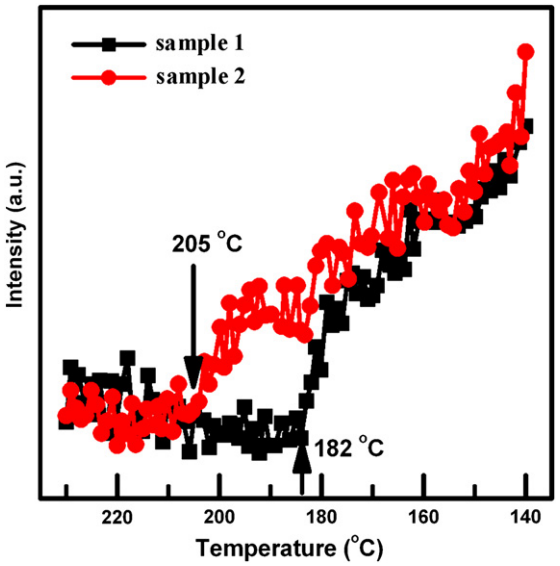

Fig. 2. Variations of SALS intensity with temperature for sample 1 and sample 2.

alloy, two thermal treatments were applied to the samples. In the first one, the samples were quenched from 230 °C and then isothermally crystallized at 132 °C. The POM micrographs of sample 1 and sample 2 after complete crystallization at 132 °C are shown in Fig. 3(a) and (b), respectively. It is found that spherulites with radiant fibrils are formed for sample 2, but the final shape of the spherulites is polygonal due to impingement. In contrast, it is hard to observe the radiant fibrils inside the spherulites of sample 1 and the spherulites exhibit a coarse structure. For both samples, there are amorphous regions between the spherulites, which are indicated by the black zones surrounding the spherulites in the micrographs.

The samples were also quenched from 230 °C and then hold at 160 °C for 60 min. At this temperature, phase separation will take place but crystallization will not occur. Subsequently, the samples were cooled to 132 °C for isothermal crystallization. The POM micrographs of sample 1 and sample 2 after this thermal treatment are shown in Fig. 3(c) and (d), respectively. It is found that for sample 2 spherulites with polygonal shape are formed. When compared with the sample 2 directly crystallized at 132 °C, the amorphous zones between the spherulites in the sample 2 crystallized after phase separation are of smaller size, leading to the narrow boundaries between the spherulites. The structure inside the spherulites of sample 2 also becomes coarser under this thermal treatment. For sample 1 the overall morphology is quite homogeneous but coarse. Spherulites can hardly be recognized because the boundaries between different spherulites nearly disappear, which are the most evident difference between sample 1 and sample 2 under this thermal treatment. Fig. 4 shows the morphological development of sample 1 during crystallization. One can see that spherulites are still formed during crystallization. Amorphous zones of small size, as indicated by the circle in Fig. 4, are formed in the crystallization frontier. During crystallization, these amorphous zones are not pushed out from the spherulites but instead are taken up into the spherulites.

The coarse structure of the spherulites is seldom reported. When amorphous components are included into the spherulites, droplet-like domains are usually observed inside the spherulites [16,27]. In order to clarify the origin of the coarse structure of the spherulites, the morphology of the PP in-reactor alloys were also examined with phase contrast optical microscopy (PCOM). Fig. 5 shows the PCOM images of both samples after different thermal treatments, respectively. It is found that, unlike in the POM images, the coarse structure of the spherulites is not evident in the PCOM images, and droplet-like domains are observed inside the spherulites. Since the coarse structure of the spherulites is observed by POM but not by PCOM, it is highly probable that the coarse structure arises from crystallization. Comparing Figs. 3 and 5, one can see that the more amorphous domains inside the spherulites, the more coarse the spherulites, indicating that the coarse structure is still related to the inclusion of the amorphous component. As a result, we speculated that the coarse structure of the spherulites is due to crystallization of the EPR-rich phase included into the spherulites. From Fig. 5, it is also observed that phase separation prior to crystallization can lead to larger size of the included amorphous domains.

3.3. SEM

POM shows that when sample 1 is subjected to phase separation prior to crystallization, the inter-spherulitic boundary can hardly be seen after completion of crystallization, but spherulites indeed are formed during crystallization. In order to observe the inter-spherulitic boundary more clearly, the samples were etched with xylene at room temperature to remove the amorphous components and were characterized with SEM. Fig. 6 shows the SEM micrographs at different scales for sample 1 quenched from 230 °C and cooled from 160 °C, respectively. It is found that even for sample 1 cooled from 160 °C the boundaries between the spherulites can still be observed after removal of the amorphous components. However, two striking differences are noticed for sample 1 subjected to two

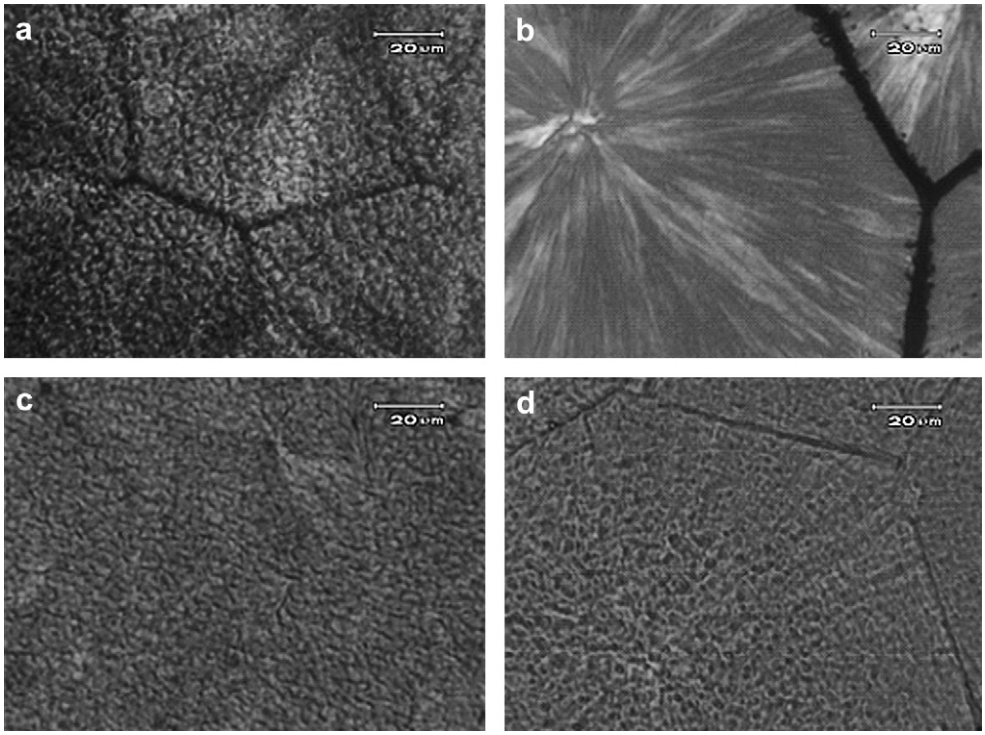

Fig. 3. POM images of sample 1 (a) and sample 2 (b) directly quenched from 230 °C to 132 °C for crystallization; sample 1 (c) and sample 2 (d) held at 160 °C for 1 h and then cooled to 132 °C for crystallization.

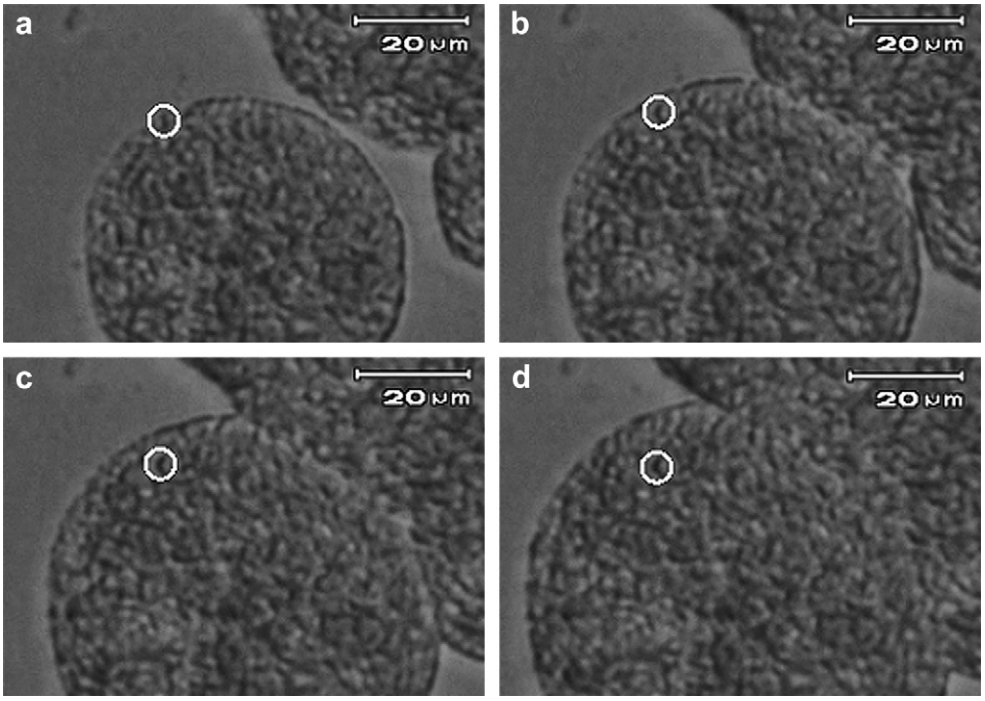

Fig. 4. Morphological development of sample 1 during crystallization at 132 °C. The sample was first held at 160 °C for 60 min and then cooled to 132 °C for crystallization. (a) 60 s; (b) 140 s; (c) 220 s and (d) 300 s.

different thermal treatments. Firstly, the sample cooled from 160 °C has much more holes inside the spherulites than the sample directly quenched from 230 °C. These holes are formed by removal of the amorphous components and should correspond to the amorphous domains. This shows that more amorphous components are included into the spherulites for the samples cooled from 160 °C, which is in accordance with PCOM observations. Secondly, the crannies between the spherulites, where the amorphous components are enriched, are much narrower in the sample cooled from 160 °C than that in the sample quenched from

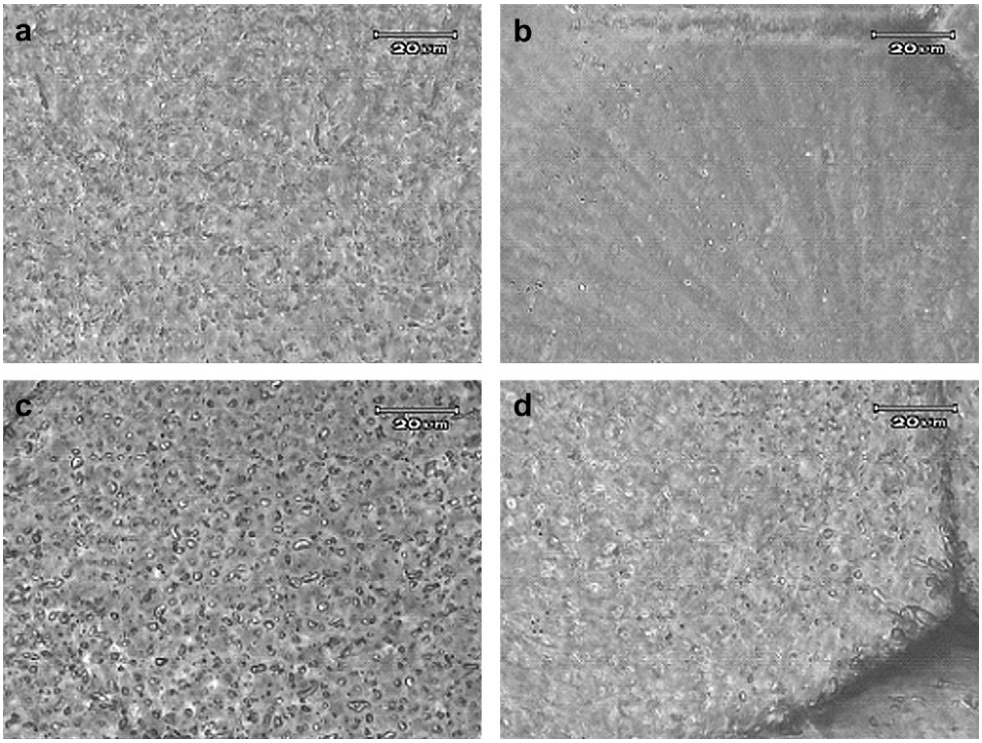

Fig. 5. PCOM images of sample 1 (a) and sample 2 (b) directly quenched from 230 °C to 132 °C for crystallization; sample 1 (c) and sample 2 (d) held at 160 °C for 1 h and then cooled to 132 °C for crystallization.

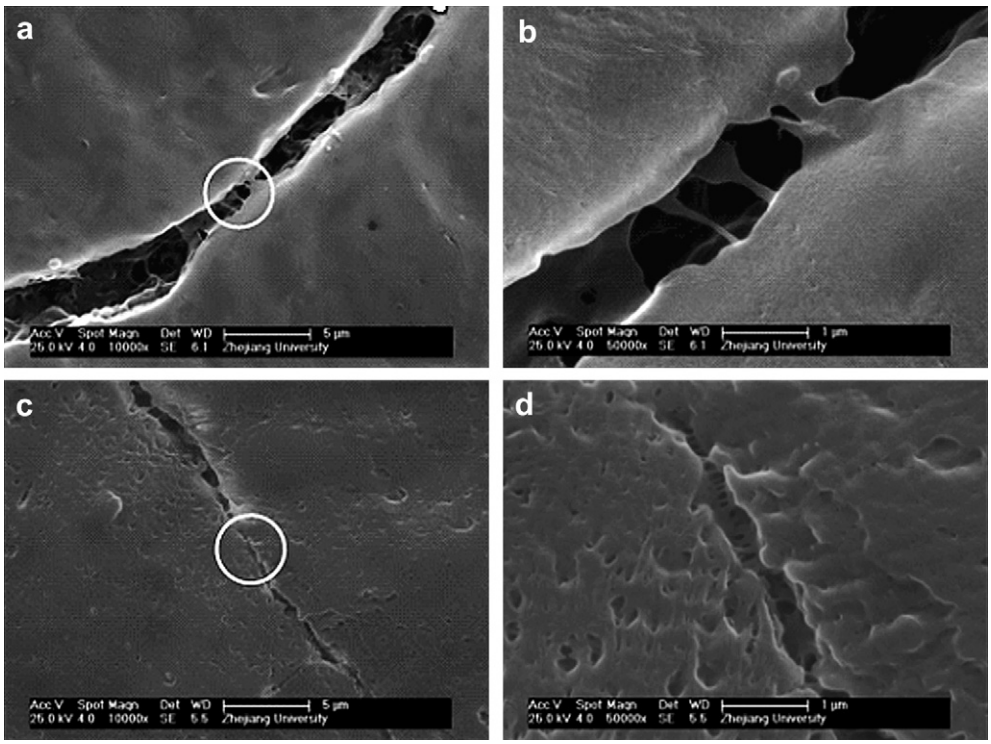

Fig. 6. SEM micrographs of sample 1 etched by xylene at room temperature (a) crystallized at 132 °C after quenching from 230 °C; (b) enlarged picture of the circled area in (a); (c) crystallized at 132 °C after held at 160 °C for 60 min; (d) enlarged picture of the circled area in (c).

230 °C. For the sample cooled from 160 °C, in the crannies there are also lots of tie fibrils connecting the adjacent spherulites, which are seldom observed in the sample quenched from 230 °C. Such morphology is clearly favorable to the mechanical properties of PP/EPR in-reactor alloys, since the boundary between the spherulites is usually the weakness of polymer materials upon tensile drawing.

4. Discussion

4.1. Phase diagram

The above results show that the inclusion of the amorphous component into the spherulites, the coarse structure within the spherulites and the inter-spherulitic boundary are affected by both phase separation and microstructure of the PP/EPR in-reactor alloys. The effect of phase separation on the inclusion of the amorphous component into the spherulites has been reported in literature, but the effect of phase separation on the latter two is rarely reported [16]. These effects can be interpreted in terms of the interplay of phase separation and crystallization. The phase diagrams of sample 1 and sample 2 are schematically depicted in Fig. 7. When the PP/EPR in-reactor alloys are quenched below the phase separation temperature, phase separation will take place first. Two phases, the PP-rich phase (denoted as concentrated phase, i.e. c phase) and the EPR-rich phase (denoted as dilute phase, i.e. d phase), will be formed upon phase separation. The compositions of the EPR-rich phase and the PP-rich phase depend on the quenching depth. In the present work the presence of the blocky component affects the compatibility between PP and EPR, thus the compositions of the PP-rich and EPR-rich phases are dependent on the volume fraction and microstructure of the blocky component. However, noting the small amount of the block component (~10 wt%) in the PP/EPR in-reactor alloys, we still treat the PP/EPR in-reactor alloys as binary blends of PP and EPR. Since the blocky component can act as compatilizer of PP and EPR and decrease the temperature of phase separation, the phase separation curve of sample 1 is narrower (i.e. smaller difference in composition between the c phase and d phase) and locates below the phase separation curve of sample 2. As a result, at the same temperature where phase separation takes place, the PP content in the EPR-rich phase follows the order: sample 1 > sample 2 (i.e. $d_2 > d_1$ and $d_4 > d_3$), and sample 1 < sample 2 (i.e. $c_2 < c_1$ and $c_3 < c_4$) in the PP-rich phase. For a sample at different phase separation temperatures, the PP content in the EPR-rich phase at high temperature is larger than that at the lower temperature (i.e. $d_4 > d_2$ and $d_3 > d_1$), and it is the reverse for the PP content in the PP-rich phase (i.e. $c_4 < c_2$ and $c_3 < c_1$).

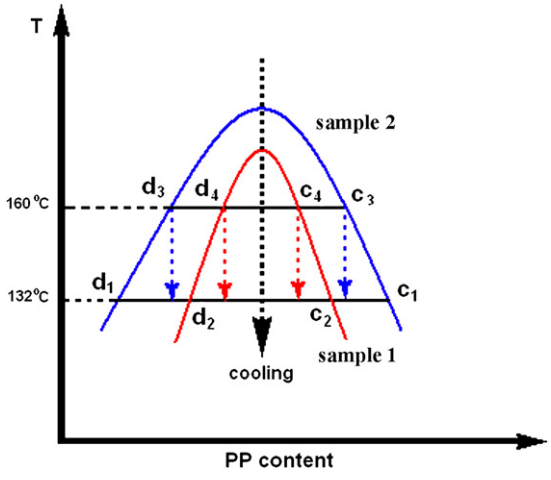

Fig. 7. Schematic phase diagrams for sample 1 and sample 2.

4.2. Inclusion of amorphous component

Based on the phase diagram schematically depicted in Fig. 7, we firstly discuss the amount of amorphous component included into the spherulites. For a system containing both crystalline and amorphous components, the amorphous component can be either included into the spherulites or excluded from the spherulites, depending on the growth rate of the spherulites and the diffusion rate of the amorphous component. If the growth rate of the spherulites is much faster than the diffusion rate of the amorphous phase, the amorphous component tends to be included into the spherulites. Otherwise, the amorphous component is excluded from the spherulites. The diffusion rate of the amorphous component is related to its viscosity, which depends on temperature and its composition. At the same temperature, the EPR-rich phase of sample 1 contains more PP than the EPR-rich phase of sample 2 ($d_2 > d_1$ and $d_4 > d_3$). Since the viscosity of PP is higher than that of EPR, the EPR-rich phase is easier to be included in sample 1 than in sample 2. As a result, more amorphous components are included into the spherulites in sample 1 than in sample 2 at the same thermal treatment. On the other hand, when the alloys are firstly held at 160 °C, phase separation will take place but crystallization will not proceed. After the phase-separated melt is quenched to 132 °C, further phase separation tends to take place in both the PP-rich and EPR-rich phases previously formed at 160 °C. However, this process may be retarded due to confinement of the pre-existed phase-separated morphology, and the inclusion of the amorphous component still depends on phase structure formed at 160 °C. Due to shallower quenching depth, the PP content in the EPR-rich phase at 160 °C is higher than that at 132 °C ($d_4 > d_2$ and $d_3 > d_1$), leading to higher viscosity of the EPR-rich phase and more EPR-rich phases included into the spherulites for the samples cooled from 160 °C.

4.3. The coarse spherulitic structure

As for the coarse spherulitic structure, it has been revealed by the POM and PCOM images that it may be due to crystallization of PP in the included EPR-rich phase. The phase diagram of PP in-reactor alloys is a little different from that of the real PP/EPR binary blends. In the real PP/EPR binary blends, the compositions of the PP-rich phase and the EPR-rich phase are highly different due to the immiscibility between PP and EPR when temperature is below the UCST. Therefore, the content of PP in the EPR-rich phase of PP/EPR binary blend is very low and PP in this phase cannot crystallize. In contrast, the phase diagram of the PP in-reactor alloy is narrower than that of the PP/EPR binary blends due to the presence of the blocky copolymer components, which means that the difference in the composition between the PP-rich phase and the EPR-rich phase is not so large and the EPR-rich phase still contains a certain amount of crystallizable PP. It should be noted that, although the EPR-rich phase also contains crystallizable PP, crystallization of the PP in the EPR-rich phase is slightly behind that in the PP-rich phase due to the lower concentration of PP in the former. Therefore, the EPR-rich phase is still amorphous immediately after crystallization of PP in the PP-rich phase. When the EPR-rich phase is included into the spherulites formed by the PP in the PP-rich phase, subsequent crystallization of PP in the EPR-rich phase is confined inside the spherulites but causes coarsening of the spherulites. The extent of coarsening of the spherulites is dependent on the composition and amount of the EPR-rich phase included into spherulites. As discussed in the above section, the EPR-rich phase of sample 2 crystallized from directly quenched melt contains the fewest PP, thus coarsening of the spherulites is the weakest. On the contrary, because the PP content in the EPR-rich phase of sample 1 cooled from 160 °C is the highest, this sample exhibits the coarse spherulite structure at the largest extent. The coarse spherulitic structure was also reported by Doshev et al. in a PP/EPR in-reactor alloy [13], in which the EPR was prepared at a high ethylene/propylene feed ratio in the second copolymerization stage. In such an alloy, the EPR should be also crystalline due to its high ethylene content.

4.4. Inter-spherulitic boundary

The gap between the spherulites is related to the amount of the amorphous components expelled from the spherulites (or the amount of the amorphous components included into the spherulites). The more the amorphous components expelled, the broader the gap. The relationship between the amount of the amorphous included into the spherulites and the thermal treatment and microstructure of PP in-reactor alloys has been discussed in previous section. On the other hand, formation of tie fibrils connecting the adjacent spherulites depends on the width of the gaps between the spherulites and the crystallizability of the components aggregating in gaps. If the gap is too wide, connections between the adjacent spherulites are difficult to form. This means the amount of the components expelled from the spherulites during crystallization should not be too high for formation such an inter-spherulitic boundary structure. Moreover, the components expelled into the gaps should also be partially crystalline, which can crystallize after formation of spherulites. Lustiger et al. used crystalline propylene–ethylene random copolymer (with an ethylene content of 5.3 mol%) or a multiblock copolymer of isotactic and atactic polypropylene to blend with isotactic PP homopolymer [27]. The crystalline random copolymer or blocky copolymer was rejected into the inter-spherulitic boundaries. Subsequent crystallization of the random copolymer or blocky copolymer connected the adjacent spherulites and enhanced the strength of the inter-spherulitic boundaries. In the present work, the crystalline component enriched in the inter-spherulitic boundaries is PP in the EPR-rich phase and is unlike to be the blocky fractions, since the overall content of the blocky fractions is very low (~10 wt%) [24]. The SEM images show that isothermal thermal treatment at 160 °C for phase separation prior to crystallization is favorable to formation of connections between the adjacent spherulites (Fig. 6). This can also be interpreted in terms of the phase diagram. Upon phase separation at 160 °C, the EPR-rich phase contains more PP than the EPR-rich phase formed at lower temperature. Since the EPR-rich phase and PP-rich phase formed at higher temperature are difficult to undergo second phase separation when they are cooled to lower crystallization temperature due to morphological confinement. The higher PP content in the EPR-rich phase leads to more EPR-rich phase is included into the spherulites (thus narrower gap between the spherulites) and stronger crystallizability of the components expelled into the inter-spherulitic boundaries. The connected spherulites were reported by Du et al. in polypropylene/poly(ethylene-*co*-octene) (PP/PEOc) in-reactor alloy as well [16]. Similarly, they found that phase separation in the melt prior to crystallization was advantageous to formation of such morphology. They attributed the connections between the adjacent spherulites to PP, though they did not show the crystallizability of the PEOc component. One difference between morphology of the PP/PEOc in-reactor alloys in literature and the PP/EPR in-reactor alloys in the present work is no coarse structure of the spherulites was observed in the PP/PEOc alloys. We speculate that PP has worse compatibility with PEOc and thus the PEOc-rich phase contains fewer PP after phase separation, leading to its weaker crystallizability. PP in the included PEOc-rich phase cannot crystallize due to confinement in the spherulites and forms droplet-like domains, but PP in the PEOc-rich phase expelled into the crannies between the spherulites still can crystallize due to less

confinement and forms tie fibrils connecting the adjacent spherulites. In contrast, for the PP/EPR in-reactor alloys containing blocky fractions in the present work, both the EPR-rich phase included into the spherulite and the EPR-rich phase expelled into the boundaries can crystallize due to its higher PP content, leading to a coarse spherulitic structure and the connecting tie fibrils between the adjacent spherulites, respectively.

5. Conclusions

Thermal fractionation reveals that the blocky components in the alloy prepared by multi-stage sequential polymerization contain more PP segments than in the alloy prepared by two-stage polymerization. This leads to the lower phase separation temperature of sample 1, thus at the same temperature the quench depth and the compositions of the EPR-rich and PP-rich phases are different for sample 1 and sample 2. The amount of the EPR-rich phase included into the spherulites depends on the PP content in the EPR-rich phase, since more PP result in higher viscosity. Coarsening of the spherulites is related to crystallization of PP in the EPR-rich phase included into the spherulites. Thermal treatment also affects the boundaries between the spherulites. Phase separation prior to crystallization is favorable to formation connections between the adjacent spherulites.

Acknowledgements

This work was support by the Special Funds for Major State Basic Research Projects (grant no. 2005CB623804) and State Key Laboratory of Chemical Engineering (No. SKL-ChE-07D01).

References

[1] Simonazzi T, Cecchin G, Mazzullo S. Prog Polym Sci 1991;16:303.
[2] Galli P, Haylock JC. Prog Polym Sci 1991;16:443.
[3] Galli P, Vecellio G. Prog Polym Sci 2001;26:1287.
[4] Galli P, Haylock JC. Makromol Chem Macromol Symp 1992;63:19.
[5] Cecchin G, Marchetti E, Baruzzi G. Macromol Chem Phys 2001;202:1987.
[6] Fu ZS, Fan ZQ, Zhang YQ, Feng LX. Eur Polym J 2003;39:795.
[7] Fu ZS, Fan ZQ, Zhang YZ, Xu JT. Polym Int 2004;53:1169.
[8] Urdampilleta I, Gonzalez A, Iruin JJ, de la Cal JC, Asua JM. Macromolecules 2005;38:2795.
[9] Chen Y, Chen Y, Chen W, Yang DC. J Appl Polym Sci 2008;108:2379.
[10] Chen Y, Chen Y, Chen W, Yang DC. Polymer 2006;47:6808.
[11] Jiang T, Chen HX, Ning YN, Kuang DT, Qu GM. J Appl Polym Sci 2006;101:1386.
[12] Tan HS, Li L, Chen ZN, Song YH, Zheng Q. Polymer 2005;46:3522.
[13] Doshev P, Lohse G, Henning S, Krumova M, Heuvelsland A, Michler G, et al. J Appl Polym Sci 2006;101:2825.
[14] Chen Y, Chen Y, Chen W, Yang D. Eur Polym J 2007;43:2999.
[15] Zhu HJ, Monrabal B, Han CC, Wang DJ. Macromolecules 2008;41:826.
[16] Du J, Niu H, Dong JY, Dong X, Wang D, He A, et al. Macromolecules 2008; 41:1421.
[17] Xu JT, Feng LX, Yang SL, Wu YN, Yang YQ, Kong XM. Polymer 1997;38:4381.
[18] Cai HJ, Luo XL, Ma DZ, Wang JM, Tan HS. J Appl Polym Sci 1999;71:93.
[19] Xu JT, Fu ZS, Fan ZQ, Feng LX. Eur Polym J 2002;38:1739.
[20] Galli P. J Macromol Sci – Pure Appl Chem 1999;A36:1561.
[21] Covezzi M, Mei G. Chem Eng Sci 2001;56:4059.
[22] Fernandes FAN, Lona LMF. J Appl Polym Sci 2004;93:1042.
[23] Santos JL, Asua JM, de la Cal JC. Ind Eng Chem Res 2006;45:3081.
[24] Dong Q, Wang XF, Fu ZS, Xu JT, Fan ZQ. Polymer 2007;48:5905.
[25] Wang LX, Huang BT. J Polym Sci Part B Polym Phys 1991;29:1447.
[26] Yokoyama Y, Ricco T. J Appl Polym Sci 1997;66:1007.
[27] Lustiger A, Marzinsky CN, Mueller RR. J Polym Sci Part B Polym Phys 1998;36:2047.
[28] Nitta K, Kawada T, Yamahiro M, Mori H, Terano M. Polymer 2000;41:6765.
[29] Xu JT, Feng LX. Polym Int 1998;47:433.
[30] Fan ZQ, Zhang YQ, Xu JT, Wang HT, Feng LX. Polymer 2001;42:5559.
[31] Fu ZS, Xu JT, Zhang YZ, Fan ZQ. J Appl Polym Sci 2005;97:640.
[32] Tanaka H, Nishi T. Phys Rev Lett 1985;55:1102.
[33] Tanaka H, Nishi T. Phys Rev A 1989;39:783.
[34] Inaba N, Sato K, Suzuki S, Hashimoto T. Macromolecules 1986;19:1690.
[35] Inaba N, Yamada T, Suzuki S, Hashimoto T. Macromolecules 1988;21:407.
[36] Crist B, Hill MJ. J Polym Sci Part B Polym Phys 1997;35:2329.
[37] Lim SW, Lee KH, Lee CH. Polymer 1999;40:2837.
[38] Wang H, Shimizu K, Hobbie EK, Wang ZG, Meredith JC, Karim A, et al. Macromolecules 2002;35:1072.
[39] Wang H, Shimizu K, Kim H, Hobbie EK, Wang ZG, Han CC. J Chem Phys 2002;116:7311.
[40] Shimizu K, Wang H, Wang ZG, Matsuba G, Kim H, Han CC. Polymer 2004; 45:7061.
[41] Wang ZG, Wang H, Shimizu K, Dong JY, Hsiao BS, Han CC. Polymer 2005; 46:2675.
[42] Zhang XH, Wang ZG, Muthukumar M, Han CC. Macromol Rapid Commun 2005;26:1285.
[43] Zhang XH, Wang ZG, Dong X, Wang DJ, Han CC. J Chem Phys 2006;125:024907.
[44] Niu YH, Wang ZG, Orta CA, Xu DH, Wang H, Shimizu K, et al. Polymer 2007;48:6668.
[45] Shimizu K, Wang H, Matsuba G, Wang ZG, Kim H, Peng WQ, et al. Polymer 2007;48:4226.
[46] Zhang XH, Man XK, Han CC, Yan DD. Polymer 2008;49:2368.
[47] Tao LY, Shangguan YG, Jiang X, Zheng Q. Acta Polym Sin 2008;48.
[48] Zuo M, Peng M, Zheng Q. Polymer 2005;46:11085.
[49] Xu JT, Ding PJ, Fu ZS, Fan ZQ. Polym Int 2004;53:1314.
[50] Chen CY, Yunus WMZW, Chiu HW, Kyu T. Polymer 1997;38:4433.
[51] Pang YY, Dong X, Zhao Y, Han CC, Wang DJ. Polymer 2007;48:6395.
[52] Seki M, Nakano H, Yamauchi S, Suzuki J, Matsushita Y. Macromolecules 1999;32:3227.